Advanced Drug Delivery Reviews 71 (2014) 86–97

Contents lists available at ScienceDirect

Advanced Drug Delivery Reviews

journal homepage: www.elsevier.com/locate/addr

Nanoprecipitation and the "Ouzo effect": Application to drug delivery devices ☆

Elise Lepeltier, Claudie Bourgaux, Patrick Couvreur

UMR CNRS 8612, Institut Galien Paris-Sud, Université Paris-Sud, France

ARTICLE INFO

Available online 30 December 2013

Keywords:
Nanoprecipitation
Ouzo effect
Nanoparticles
Nucleation and growth
Terpenoid prodrug
Squalenoylation

ABSTRACT

Biodegradable nanocarriers such as lipid- or polymer-based nanoparticles can be designed to improve the efficacy and reduce the toxic side effects of drugs. Under appropriate conditions, nanoprecipitation of a hydrophobic compound solution in a non-solvent can generate a dispersion of nanoparticles with a narrow distribution of sizes without the use of surfactant ("Ouzo" effect). The aim of this review is to present the main parameters controlling the nucleation and growth of aggregates in a supersaturated solution and the characteristics of the obtained nanoparticles. The importance of the kinetics of mixing of the solution containing the hydrophobic compound and the non-solvent is highlighted. Illustrative examples of polymeric nanoparticles for drug delivery or terpenoid-based nanoprodrugs obtained by nanoprecipitation are reported.

Contents

1. Introduction

Nanocarriers can provide a crucial advantage to various drugs and therapeutic biological molecules such as nucleic acids and proteins by improving their efficacy and reducing potential toxic and side effects. Biodegradable nanoparticles (NPs) offer possibilities to protect therapeutic agents against degradation, to control their release, to overcome biological barriers and to target specific sites of action [1–7]. The physicochemical properties of nanoparticles, such as composition, size, morphology and surface properties, can impact the biodistribution and pharmacokinetics of drugs by modifying interactions with the biological environment [8–15].

Among these characteristics, nanoparticle size is a crucial parameter, especially for intravenous administration, since it strongly influences the adsorption of the plasma proteins (opsonins), which results in recognition of the nanoparticles by the macrophages of the reticuloendothelial system (RES) and rapid clearance from the bloodstream. It has been shown that clearance of the smaller particles (~80 nm) was slower than that of the bigger particles (~200 nm), due to a lower quantity of adsorbed plasma proteins. Additionally, filtration of NPs by the spleen and trapping in the hepatic parenchyma also depended on size. Regarding cancer therapy, nanocarriers can take advantage of the so-called enhanced permeation and retention effect (EPR): the leaky vasculature of some solid tumors, in combination with a weak lymphatic drainage,

☆ This review is part of the *Advanced Drug Delivery Reviews* theme issue on "Editor's Choice 2014".

0169-409X/$ – see front matter
http://dx.doi.org/10.1016/j.addr.2013.12.009

may result in a selective accumulation of colloidal carriers in the target tissue [16,17]. The effective pore size in the endothelium of the blood vessels in many human tumors has been reported to range from 200 nm to 600 nm [18,19]. Therefore, there is a consensus that particles should measure less than 200 nm and preferably less than 100 nm to benefit from the EPR effect. On the other hand, in healthy tissues, a diameter larger than 10 nm usually hinders the diffusion of the NPs through the vessel endothelium, minimizing side effects. At the cellular level, the mechanisms of NP internalization, either phagocytosis or endocytosis, are also influenced by size [8–10]. Therefore, the size and the size distribution of NPs need to be accurately controlled for efficient and safe drug delivery.

Among the different methods described for NP preparation [20–22], the solvent displacement method (or solvent shifting, or nanoprecipitation) is a straightforward and fast process differing from emulsion-based methods (emulsification–diffusion, emulsion–evaporation and salting-out techniques) in that no precursor emulsion is required. In practice, the hydrophobic solute (polymer or lipid molecules) is first dissolved into a polar organic solvent (usually ethanol, acetone or THF). This solution is then added to a large amount of a non-solvent (generally water) of the solute with which the polar solvent is miscible in all proportions. The mixed binary solution becomes a non-solvent for the hydrophobic molecules and the system evolves towards phase separation, leading to the formation of particles of the hydrophobic solute. The organic solvent can then be removed by evaporation. This methodology is easy but the main practical limitation lies in possible flocculation of particles and formation of large aggregates.

Under appropriate conditions, this process instantaneously generates a dispersion of small droplets or nanoparticles with a narrow unimodal size distribution in the 50–300 nm range. This spontaneous emulsification process, which does not require surfactant, has been named the "Ouzo effect" by Vitale and Katz from the generic example of the Greek beverage [23]. The major components of Ouzo (Pastis in France) are water (~55%), alcohol (~45%) and trans-anethol (~0.2%), a water-insoluble oil extracted from anise seeds. Upon dilution with water, anethol is no longer solubilized in the water/ethanol mixture. Ouzo becomes spontaneously milky due to the formation of long-lived metastable oil droplets which scatter visible light. Reexamining publications (until 2005) dealing with the preparation of various nanoparticles or nanocapsules via the solvent displacement method, Ganachaud and Katz suggested that the formation of these dispersions was triggered by the Ouzo effect [24]. Small hydrophobic organic molecules and lipids or polymers can act similar to oil molecules and the Ouzo effect can therefore lead to the formation of nanoparticles.

Numerous studies were intended to identify the most pertinent experimental parameters controlling the size and polydispersity of NPs. Some investigations have focused on the phase diagrams of the ternary systems, solute/solvent/non-solvent, in order to determine the region of the composition map where only nanoparticles are obtained (Ouzo region). Attempts have been made to clarify the mechanisms controlling the kinetics of formation and the characteristics of the obtained nanoparticles. This knowledge is of prime importance for preparing monodisperse nanoparticles in an efficient and reproducible manner, using a rational approach instead of a trial-and-error process.

The purpose of this review is to present recent advances in the knowledge of the formation of organic nanoparticles using the solvent displacement method with emphasis on drug delivery applications.

2. Brief theoretical background

When a solution comprised of a hydrophobic solute in a polar, water miscible, solvent is mixed with a large amount of water, the concentration of the solute in the resulting solution exceeds its thermodynamic solubility limit. The ratio of the actual solute concentration to the equilibrium solubility defines the supersaturation (S) of the solution. On the phase diagram of the ternary system solute/solvent/non-solvent, the binodal curve corresponds to the miscibility limit as a function of composition, whereas the spinodal curve defines the limit of thermodynamic stability. The system evolves by nucleation of solute particles (or droplets) in the metastable region of the phase diagram (between the binodal and spinodal curves) or by spinodal decomposition, i.e. spontaneous growth of concentration fluctuations, in the area delimited by the spinodal [25].

The classical nucleation theory (CNT) is the most widely used model to explain homogeneous nucleation in the metastable region. When a critical supersaturation is reached, nuclei form spontaneously from small local fluctuations in the concentration of solute molecules. CNT assumes a globular shape for the nuclei and a constant surface tension independent of the size of the nuclei. The free energy of formation of a nucleus of radius r is thus given by:

$$\Delta G = 4\pi r^2\gamma + 4/3\pi r^2 \Delta g_v$$

where γ is the surface tension and Δg_v the difference in free energy per unit volume between the two phases. The two terms are of opposite sign so that ΔG goes through a maximum when r varies.

The critical nucleus radius r*, corresponding to the maximum of the free energy, is given by:

$$r_* = -2\gamma/\Delta g_v$$

Particles with a radius smaller than the critical nucleus radius r* vanish, whereas larger particles are stable and can grow further.

The instantaneous nucleation rate and the critical nucleus radius are linked to the supersaturation (S) of the solution and to the thermodynamic properties of the particles/solution interface through γ. The nucleation rate varies as $\exp(-\gamma^3 / k^3T^3(\log S)^2)$ and r* is proportional to $(\gamma/kT \log S)$. The nucleation rate and critical nucleus radius are therefore extremely sensitive to supersaturation. At low supersaturation few stable nuclei are formed whereas high supersaturation yields a large number of very small nuclei.

It should be emphasized that, in the case of nanoprecipitation, homogeneous supersaturation requires that the mixing of the aqueous and organic phases, and the associated molecular diffusion of components, are extremely rapid as compared to the rate of nanoparticle nucleation. Particles are then assumed to grow from a single batch in which solute molecules are randomly dispersed.

Nuclei which exceed the critical size can grow further, by sticking other solute molecules from the surrounding solution, until the concentration of the still-dissolved solute has decreased to the equilibrium concentration. When the growth of particles is limited by diffusion of the solute molecules to the nucleus surface, their rate of growth depends on the supersaturation and on the diffusion coefficient (D) of the solute molecules. Beside this diffusion limited growth process, diffusion limited cluster–cluster aggregation (DLCA) may occur. When the number of nuclei is very high, growth occurs mainly through random collisions of existing particles. The probability of collision is proportional to the square of the number of particles and it is assumed that each collision causes aggregation of the two particles involved. Upon encounter, soft NPs rearrange to form dense structures, often spherical. The average size is predicted to increase linearly with time. It is expected that very high supersaturation favors the DLCA mechanism whereas at low supersaturation, nucleation and growth is the dominant mechanism [26] (Fig. 1).

Regarding the size distribution of NPs, the separation of nucleation and growth in time is a key for the formation of NPs with low polydispersity [27,28]. A single nucleation burst is required, which may be achieved by processes with very short mixing times to ensure uniform

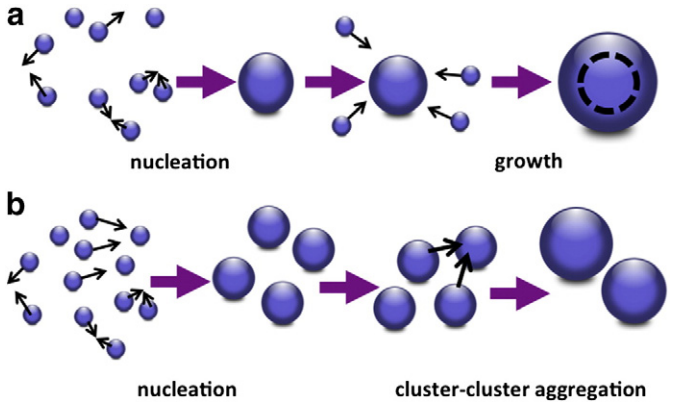

Fig. 1. Schematic description of (a) nucleation and diffusion limited growth mechanism, (b) diffusion limited cluster–cluster aggregation.

supersaturation. Nucleation may be followed by the diffusion limited growth of nuclei. It has been shown that a narrow size distribution of NPs may also be induced by coalescence of small nuclei [29–31].

Ostwald ripening (OR) is a potential mechanism involved in further particle (or droplets) growth, on a longer time scale [32]. It consists of the growth of the larger particles at the expense of smaller ones, resulting from the diffusive transport of dissolved solute through the continuous phase. The reduction of the interfacial energy term favors this process. This leads to a reduction in particle number as small particles disappear. Solubility and diffusion coefficient of hydrophobic solute in the continuous phase, and surface tension between aggregates and solution are the main parameters involved in Ostwald ripening. They are temperature dependent. A very low solubility of the hydrophobic solute in water and/or homogeneously sized particles opposes Ostwald ripening.

To summarize, the values of supersaturation (S), interfacial tension (γ) and diffusion coefficients of the solute molecules and clusters during the different stages of nucleation, growth and Ostwald ripening of particles should influence their final concentration, size and polydispersity.

In a small domain of composition of the ternary hydrophobic solute/solvent/water system, the "Ouzo domain", nanoprecipitation yields a dispersion of nanoparticles (or droplets) exhibiting a narrow size distribution whereas, beyond the Ouzo boundary, the solvent displacement process generates both nanoparticles and larger aggregates. Bimodal NP size distributions can be observed. The "Ouzo domain" is a narrow domain between the binodal and spinodal curves, corresponding to low hydrophobic solute concentrations and solvent/water ratios [33] (Fig. 2).

The Ouzo effect has been analyzed in details in model divinyl benzene (DVB)/ethanol/water and in trans-anethol (*t-A*)/ethanol/water systems [23,34–38]. It was found that the mean DVB droplet diameter was primarily a function of one parameter, the excess oil-to-solvent ratio, "excess oil" referring to the concentration of oil in excess of its saturation concentration in the solvent/water continuous phase. Increasing the excess oil-to-solvent ratio caused the mean droplet diameter to increase [23]. Regarding trans-anethol (*t-A*)/ethanol/water system, NMR spectroscopy has revealed that the spontaneous emulsification of *t-A* in water began with the formation of very small aggregates (~2 nm diameter). A very slow exchange between free *t-A* molecules in the aqueous phase and *t-A* molecules within the aggregates was observed. Rapid coalescence of these aggregates gave rise to larger droplets (~μm), responsible for the cloudy aspect of the emulsion, which have been investigated using dynamic light scattering (DLS) and small-angle neutron scattering (SANS). Further growth of the droplets occurred via Ostwald ripening, on a longer time scale, thus ensuring

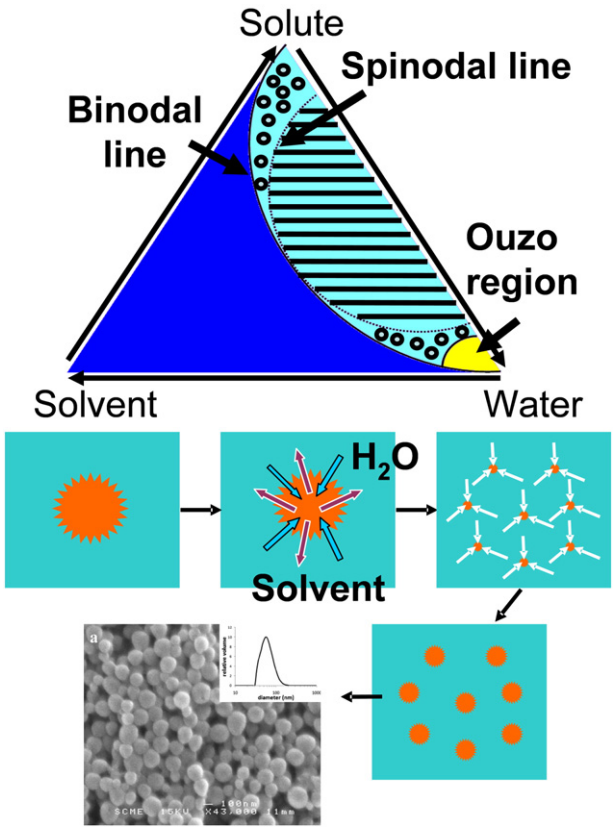

Fig. 2. Phase diagram of the ternary hydrophobic solute/solvent/water system (top, reprinted from [33]) and schematic description of the liquid–liquid nucleation process or Ouzo effect (bottom, adapted from [24]): the rapid dispersion within water of the droplets of the organic solution containing the hydrophobic oil is followed by inter-diffusion of solvent and water, leading to supersaturation of oil and nucleation of small oil droplets. Droplet growth stops when the aqueous phase is no longer supersaturated with oil. At the end of the process, the oil droplets are dispersed in the aqueous phase. A SEM photograph of nanoparticles of PMMA obtained by nanoprecipitation in the Ouzo domain is presented (reprinted from [26]).

the long life of the emulsion. OR was delayed by the homogeneous size of the droplets, the very low solubility of oil in water and the low interfacial tension of *t-A* droplets in ethanol/water mixtures. Moreover, the formation of an adsorbed layer of ethanol on *t-A* droplets could stabilize them, as suggested by Monte-Carlo simulations [33].

Taken together, observations were consistent with homogeneous liquid–liquid nucleation of the droplets and emphasized the importance of Ostwald ripening. However, the factors involved in the growth and stability of these spontaneous droplets are not fully understood.

3. Stabilization of nanoparticles

The stabilization of primary NPs is critical for maintaining small NPs. Slow processes occurring on a longer time scale, such as Ostwald ripening and/or further aggregation of NPs, may lead to large polydisperse particles. The removal of the organic solvent from the aqueous phase may reduce Ostwald ripening, thus enhancing NP stability [39]. The aggregation of the NPs may be prevented by the presence of additives such as a low molecular weight surfactant, an amphiphilic polymer, a polyelectrolyte or a polysaccharidic polymer like dextran, adsorbed or anchored at the NP surface. To stabilize the particles, the nanoprecipitation may therefore be carried out in the presence of a small quantity of a stabilizer. The stabilizer is usually not needed if NPs display hydrophilic moieties or non zero zeta potential [40,41]. Interestingly, Roger et al. have shown that aggregation of soft polymeric

NPs limited by long-range electrostatic repulsion between charged NPs may lead to the decrease of the NPs polydispersity. Indeed, the size-dependent repulsive potential favored encounters involving a large NP and a small one rather than two large NPs [42]. Moreover, the aggregation of NPs may be limited by the presence of additives that increase the viscosity of the continuous medium and lower the diffusion rate of clusters.

Nature and properties of the stabilizer affect NP size, size distribution and colloidal stability. Zhu et al. have compared the influence of the adsorption of three polyelectrolytes, ε-polylysine, poly(ethylene imine) (PEI) and chitosan on the stability of hydrophobic β-carotene NPs. High molecular weight PEI and chitosan, able to provide both steric and electrostatic stabilization, yielded the smallest NPs and had the best stabilizing effect [43]. NPs are most frequently stabilized with amphiphilic diblock copolymers which are either added to the aqueous phase, such as water dispersible polypropylene oxide–polyethylene oxide block copolymers (Pluronics® or Poloxamers®), or dissolved in the organic solvent, such as PEGylated poly(lactic-co-glycolic acid) (PLGA-b-PEG). It has been found that some copolymer chains could be kinetically trapped inside the NP core when NPs were formed by fast precipitation (flash nanoprecipitation) of an organic solution containing both hydrophobic molecules (β-carotene) and the copolymer. The impact of four widely used copolymers on β-carotene NPs has been systematically investigated and the size and stability of NPs related to the properties of the different hydrophobic blocks (glass transition temperature Tg, ability to crystallize and solubility parameter). The best stabilizing effect was obtained with PLGA-b-PEG which displays a non crystallizable hydrophobic block with high Tg [44].

When the NP growth is stopped by adsorption of additives, the concentration of additive and the relative time-scales of the different processes involved in NP formation are expected to be of primary importance in determining their final size. This was underlined by Lannibois et al. who studied the precipitation of hydrophobic molecules (cholesteryl acetate) in water in the presence of an added amphiphilic diblock copolymer made of a styrene block (molecular weight 1000) and an oxyethylene block (molecular weight 1000) (PS-PEO) [45]. They were both dissolved in acetone and the solution was mixed with a large excess of water. Cholesteryl acetate being nearly insoluble in water, aggregates formed immediately and grew through a DLCA mechanism, as suggested by the variation of the average NP volume versus cholesteryl acetate concentration. A stable dispersion was obtained when the surface of NPs was fully covered by a monolayer of surfactant. The final average NP size depended on the concentrations of hydrophobic (C_H, g/g) and surfactant molecules (C_S, g/g). For a given C_S/C_H ratio (e.g. $C_S/C_H = 1$), the NP volume increased linearly with the initial concentration of hydrophobic molecules in acetone (from $C_H = 10^{-4}$ g/g to $C_H = 10^{-2}$ g/g). The evolution of the NP volume with C_S/C_H ratio showed that, at high surfactant concentrations, the NP sizes were larger than those anticipated if all surfactant molecules had been adsorbed. Only a fraction of the copolymer was effective in controlling aggregation. It was found that part of the copolymer formed micelles in water. Experiments involving the hydrophobic hexadecane and the $C_{12}E_5$ surfactant confirmed the existence of two regimes. At moderate surfactant/hydrophobic solute ratios, all surfactant molecules coated the surface of the droplets but aggregation yielded rather large particle sizes. At high C_S/C_H ratios the aggregation was stopped at an earlier stage but part of the surfactant remained in water. Therefore, attempts to obtain smaller and smaller NPs by adding increasing amounts of surfactant should fail at some point (Fig. 3).

These experimental results could be explained by comparison with numerical simulations of the competition between aggregation of hydrophobic molecules and adsorption of surfactant. Two different power laws were evidenced in the log–log plot of the NP volume V_{av} as a function of the C_S/C_H ratio, accounting for the two regimes in the use of surfactant molecules. The exponent measured at low C_S/C_H ratios

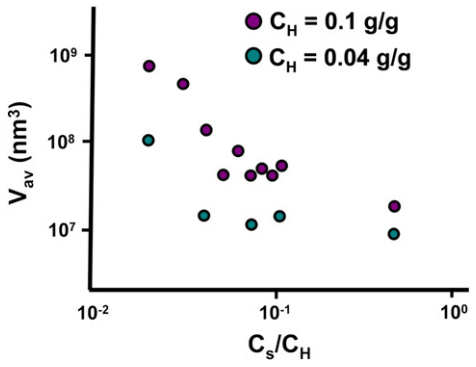

Fig. 3. Effect of surfactant ($C_{12}E_5$)/hydrophobic solute (hexadecane) ratio C_S/C_H on the average volumes V_{av} of hexadecane droplets in water. Hexadecane and $C_{12}E_5$ were both dissolved in acetone and the solution was mixed with a large amount of water. For each set of data the concentration of hexadecane, C_H, in acetone was kept constant. The evolution of V_{av} as a function of C_S/C_H shows the existence of 2 regimes (adapted from [45]).

was close to the theoretical value of -3 ($V_{av}\,\alpha\,[C_S/C_H]^{-3}$), corresponding to all surfactant molecules adsorbed on the surface of growing NPs, whereas it was about -1.3 at high C_S/C_H ratios. The influence of the time delay between aggregation of hydrophobic solute and adsorption of surfactant was also investigated. Aggregation was allowed to proceed unimpeded for a time τ before adsorption of the surfactant began. For a constant C_S/C_H ratio (e.g. $C_S/C_H = 4$), the NP size was determined by the initial concentration of hydrophobic molecules (C_H) and by the value of this time delay τ. For $\tau = 0$ the NP volume increased slightly with C_H. In the limit of long time delays, the NP volume increased linearly with the initial concentration of hydrophobic molecules, reflecting the experimental results.

4. Solvent elimination

Removal of solvent from the NP suspensions is important for biomedical applications. As the solvent is miscible with both the hydrophobic molecules and water, NPs prepared by nanoprecipitation should contain a fraction of solvent, determined by the partition coefficient, in equilibrium with solvent in the aqueous phase. As an example, the partition coefficient of ethanol, defined as the ratio of the weight fraction of ethanol in water to that in the organic phase, was reported to be 6.9 for DVB [23]. In some cases, the suspensions are dialyzed against water or buffer [46]. The usual solvents (ethanol, THF, and acetone) are generally removed by evaporation under reduced pressure since their boiling points are lower than that of water. Kumar and Prud'homme have recently designed an efficient and scalable process of solvent removal based on flash evaporation. It consists of partial vaporization of a preheated liquid stream sprayed inside a vacuum chamber. It has been shown that THF concentration was reduced by over 95% after two flash stages, dropping from ~10 to less than 0.5 wt.% in residual liquid [39]. A new approach has also been proposed recently, using a supercritical CO_2 extraction process for an effective elimination of acetone and acetone/ethanol mixtures from suspensions of polymeric nanoparticles. Lower quantities of residual solvent (few ppm) were measured with respect to the usual evaporation process [47]. Despite its practical importance, the issue of residual solvent in NP suspensions was seldom addressed.

5. Experimental processes of mixing

Nucleation in the metastable region of the phase diagram or spinodal decomposition in the unstable region should depend on the mixing conditions of the organic solution containing the hydrophobic component and water. Specifically, the local instantaneous supersaturation, resulting from interdiffusion of solvent and water in small droplets

of the organic solution dispersed within the aqueous phase, is expected to depend on the mixing process. The nucleation and growth of particles may be initiated within the droplets before complete mixing can occur. When nanoprecipitation is performed by dropwise addition of the organic solution into the aqueous phase, a continuous change in the composition of the solute/solvent/ non-solvent mixture is induced. Different experimental devices have therefore been implemented to achieve a better control of the mixing of the two phases (Fig. 4). In a stopped-flow setup, defined volumes of the two phases are rapidly mixed and introduced into a cell where NPs grow. In a continuous flow apparatus converging channels carry the organic solution and water which are mixed at the T (or Y)-junction and then flow out through the exit channel where nanoprecipitation takes place. The suspension of nanoparticles is recovered at the outlet of this channel. Several types of mixers have been inserted into these devices, e.g. a millifluidic or microfluidic mixer or a confined impinging jet mixer, to ensure a fast and reproducible mixing of the two solutions [28,40,48–51]. Depending on the mixing conditions, the mixing may be laminar or turbulent and the mixing time varies. Mixing times of less than 1 ms have been achieved with a microfluidic device using hydrodynamic flow focusing where the organic polymer solution was squeezed into a narrow stream flowing between two water streams. The thin width of the focused stream enabled rapid interdiffusion of solvent and water [49]. Numerical simulations of the fluid dynamics have been recently performed to evaluate the mixing efficiency for a high pressure interdigital multilamination micromixer [52]. In this device, thin layers of polymer solution and water are alternatively stacked before entering a flow-focusing section, where their width is decreased. The water-to-solvent ratio R is set by their relative flow rates. The mixing efficiency was defined as the fluid volume fraction in the flow-focusing section where nucleation was possible due to supersaturation. Simulations indicated that increasing the flow rates while keeping R constant increased the mixing efficiency. Smaller polymeric NPs were obtained experimentally. Nanoprecipitation was therefore determined by the hydrodynamics within the micromixer, for given water-to-solvent ratio and initial concentration of polymer in solvent.

In a pioneering work, Horn and co-workers developed a continuous mixing chamber process for the industrial production of nanodispersed carotenoid hydrosols [25]. These tetraterpenes, displaying various moieties at the chain ends, are insoluble in water and poorly soluble in lipids. In this process, a solution of a carotenoid in a water miscible solvent, usually ethanol, was nanoprecipitated by turbulent mixing with an aqueous phase containing dissolved gelatin that provided colloidal stability to the NPs. The resulting monodisperse NPs exhibited a core/shell structure with a carotenoid core surrounded by a gelatin shell. In a recent review, D'Addio and Prud'homme have discussed the formation of drug nanoparticles by rapid solvent shifting [48]. They have pointed out the advantages of the continuous confined jet mixers which can scale up from laboratory experiment to industrial production.

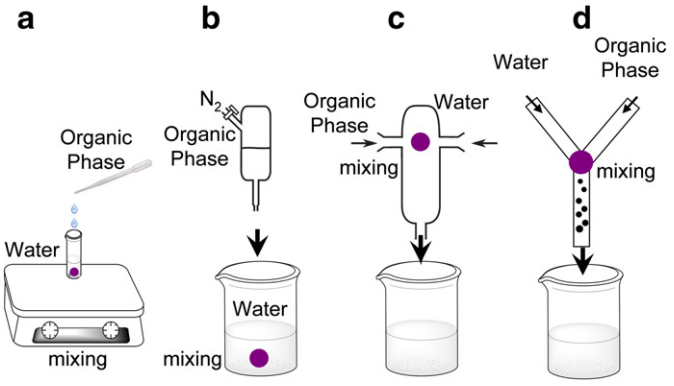

Fig. 4. Different nanoprecipitation devices: (a). Scheme of a dropwise process, (b). Pressure driven injection device (adapted from [53]), (c). Impinging jet mixer (adapted from [40]) and (d). Y-junction in a continuous-flow nanoprecipitation device.

Stopped-flow or continuous flow devices may be coupled with measurement techniques such as synchrotron small-angle X-ray scattering (SAXS) to follow the early stages of nanoparticles formation. Kinetic studies of the formation of nanoparticles may enable to assess nucleation and growth models. Hitherto, almost all time-resolved studies of the formation of colloidal particles in liquid media dealt with inorganic NPs, such as gold NPs. In many experiments, the supersaturation of the inorganic precursor was induced by chemical reactions occurring upon rapid mixing of two solutions [28,30,31,54]. For instance, gold NPs could be obtained from the reduction of an aqueous solution of gold salt by ascorbic acid. This chemical reaction was analogous to the rapid decrease of solvent quality in nanoprecipitation process.

6. Nanoprecipitation of small organic molecules: can spinodal decomposition play a role?

The formation of amorphous NPs from small organic molecules (cholesteryl acetate, β-carotene, dyes…) for which the crystalline phase is the thermodynamically stable phase seems to be a common feature of the nanoprecipitation of low molecular weight compounds at high supersaturation. The mechanism behind is a subject of debate. According to Lannibois et al., amorphous cholesteryl acetate aggregates were due to residual solvent and water plasticizing the NPs [45]. The amorphous state of polyelectrolyte stabilized β-carotene NPs obtained by very fast precipitation was considered to result from kinetic barriers to crystallization. The β-carotene molecules did not have enough time to align and pack tightly [43]. However, Brick et al. suggested that the preferential formation of amorphous dye NPs was consistent with a spinodal decomposition process, following counterdiffusion of solvent and water in organic solution droplets. Phase separation could occur faster than crystallization [55].

According to Horn and Rieger, either homogeneous nucleation or spinodal decomposition can occur in most systems containing low molecular weight hydrophobic solutes, depending on solute supersaturation. Nucleation and growth can take place at moderate solute supersaturation whereas at high supersaturation spinodal decomposition can occur. The borderline between the metastable region and the spinodal region can be crossed during mixing of solvent and water, especially if the organic solution droplets in water are small and the diffusive transport of solvent and water is fast [25,55]. The current mechanism of nanoprecipitation is very difficult to unravel because of the short time scales and space scales involved. The aggregates formed at the very beginning of the process can evolve rapidly. Attempts have been made to observe the early stages of quinacridone and boehmite particle formation using transmission electron microscopy. Samples were quenched immediately (~10 ms) after establishment of supersaturation [56].

The formation of amorphous NPs upon nanoprecipitation opens new perspectives for the preparation of poorly soluble pharmaceutical compounds NPs with enhanced bioavailability, due to increased dissolution rate.

7. Nanoprecipitation of polymers: which parameters matter?

Since the pioneering work of Fessi et al. numerous nanoparticles, prepared with different polymers and solvents, have been obtained using the solvent displacement method [22,57,58]. The most widely used polymers were poly(lactic acid) (PLA), poly(lactide-co-glycolide) (PLGA), poly(alkyl cyanoacrylate) (PACA) and poly(ε-caprolactone) (PCL), and the corresponding copolymers with poly(ethylene-glycol) (PEG) moiety, which fulfill drug delivery device requirements of biodegradability, biocompatibility and absence of immunogenicity (Fig. 5). Systematic experiments have provided information regarding the location of the "Ouzo region", where only nanoparticles are obtained, and identified the relevant parameters controlling the yield of production,

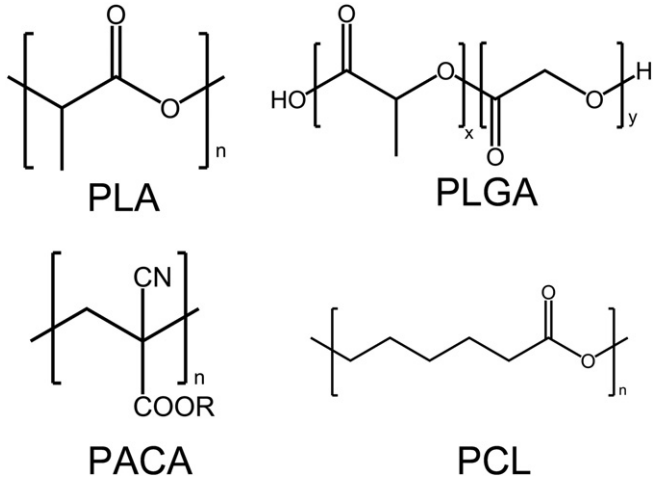

Fig. 5. Chemical formula of several polymers widely used to produce nanoparticles by solvent displacement method: PLA (poly(lactic acid)), PLGA (poly(lactide-co-glycolide)), PACA (poly(alkyl cyanoacrylate)) and PCL (poly(ε-caprolactone)). n, x and y correspond to the number of respective monomers.

size and polydispersity of nanoparticles. The respective influences of solvent/water ratio, polymer/solvent ratio, polymer molar mass, nature of the solvent, interfacial tension and solvent/non-solvent mixing time have been investigated.

It has been shown that, at the Ouzo boundary, the initial weight fraction of polymer decreased exponentially with increasing solvent/ water ratio: the log [weight fraction of polymer in solvent] was a linear function of [solvent/water ratio]. This trend was evidenced in several systems, e.g. poly(methymethacrylate) (PMMA)/ acetone, PCL/acetone and PLGA/acetone [26,59,60]. The relevant parameters for the Ouzo boundary are, therefore, the initial concentration of polymer in organic solvent and the solvent/water ratio. As pointed out by Aubry et al., the Ouzo limit is actually different from both the binodal and the spinodal lines [26]. Optimal conditions for nanoprecipitation were achieved when the polymer was dissolved in a theta solvent and when the solution was in the dilute regime, so that the polymer coils did not overlap. Nanoparticles with a smaller mean size and lower polydispersity in addition to a better production yield were obtained. Conversely, above a critical polymer concentration in solvent, large aggregates were formed in addition to the NPs, even when increasing the water/solvent ratio [21,61].

In the PMMA/acetone, PCL/acetone and PLGA/acetone systems the influence of the initial concentration of polymer in the organic solvent on the mean particle size has been investigated [26,60,62]. Nanoprecipitation was performed by adding in one shot a large volume of aqueous phase into the organic phase (PMMA/acetone) or by injection at controlled flow rate of the organic solution into water (PLGA/acetone and PCL/acetone). Increasing the polymer concentration resulted in an increase in mean particle size. In the Ouzo region, the mean particle diameter varied as a power law of polymer weight fraction. The log–log representation of the mean diameter of PMMA and PCL NPs as a function of initial polymer weight fraction or concentration (mg/mL) was a straight line with slope close to 1/3, indicating that the volume per particle was proportional to the concentration of polymer in the initial solution. Kissel and co-workers have shown that the log–log curves of PLGA nanoparticles obtained for different weight fractions of acetone (fa = 0.1, fa = 0.2, fa = 0.3) superimposed when the mean diameter of nanoparticles was redrawn as a function of (fp/fa) (fp was the final weight fraction of PLGA) [60]. This suggested that the mean size of the formed nanoparticles depended only on the ratio of polymer to solvent fp/fa. The slope of the resulting log–log curve was 1/3 (Fig. 6).

Experimental data dealing with the influence of the polymer molar mass on nanoprecipitation are rather scarce. Legrand et al. have studied a homologous series of poly(lactic acid) polymers (PLAs) with molar masses from 22 600 g/mol to 124 800 g/mol. At low polymer concentration (5 mg/mL), the molar mass had little influence on the yield of nanoparticles formed when acetone was the solvent. However, for molar masses higher than 32 100 g/mol, the mean hydrodynamic

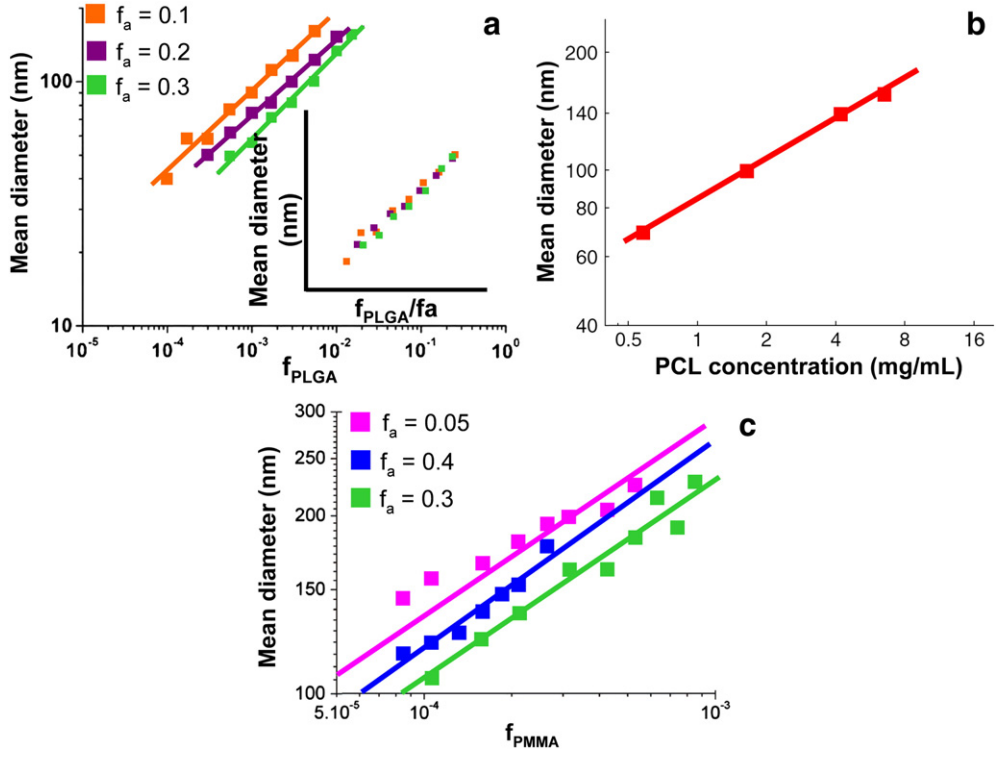

Fig. 6. Mean diameter of polymeric nanoparticles as a function of the final weight fraction of polymers, f_{PLGA} (a) and f_{PMMA} (c), for different weight fractions of acetone, or as a function of the concentration of PCL in acetone (b). (c): Symbols are experimental data and lines are theoretical fits according to a nucleation–aggregation mechanism. Insert of (a): mean diameter of PLGA nanoparticles as a function of the ratio f_{PLGA}/fa (adapted from [26,60,62]).

diameter of NPs increased with increasing molar mass (from less than 100 nm at 22 600 g/mol and 32 100 g/mol to about 250 nm at 124 800 g/mol). These results were tentatively correlated to the lower amphiphilic character of long PLA chains since chain ends bear a polar group [61]. On the other hand, Kissel et al. did not observe a significant difference in particle size upon varying the molar masses of PLGA (12, 34, and 48 kDa) dissolved in acetone at different concentrations (5–15 mg/mL), although the viscosities of the polymer solutions differed substantially as a function of the molar mass [60]. The same results have been found for nanoparticles of PCL with molar mass varying from 2 to 80 kg/mol [62].

The influence of the interfacial tension between the solvent and the non-solvent on NP formation has been investigated by Kissel et al. [60]. They injected PLGA dissolved in acetone into either pure water or a mixture of water and acetone, having a lower interfacial tension than pure water. No significant differences in NP size were seen, as would be expected if nanoprecipitation was mainly governed by the so-called Marangoni effect, described as "surface tension-driven flow". The Marangoni effect has been assumed to induce turbulences at the interface of the solvent and the non-solvent, resulting in the fingering of the organic phase into the aqueous phase and then formation of smaller and smaller droplets. In that case, the formation of particles should be due to the aggregation of the chains present in the droplets [22]. Other investigators also pointed out that interfacial tension and mechanical turbulence were not the driving forces for spontaneous emulsification [23,37].

The mean size of NPs was found dependent on the nature of the solvent used to solubilize the polymer. For instance, whatever the polymer, the NPs obtained from acetone solutions were always smaller than those prepared from THF under the same conditions. It has been suggested that the lower viscosity and higher diffusion coefficient of acetone in water, compared to THF, should promote faster mixing of solvent and water, resulting in more uniform supersaturation leading to smaller particles [60,61]. Cheng et al. have investigated the impact of solvent miscibility with water on PLGA–PEG NP size, using four solvents (acetonitrile, THF, acetone and DMF). They observed a decrease in the mean NP size when solvent/water miscibility increased [63].

The mixing time of the organic solution containing the polymer with the aqueous phase is a crucial parameter. It has been shown that faster mixing led to a reduced mean size of the resulting nanoparticles [40,49,52]. Outstanding results have been obtained by Johnson and Prud'homme whose experiments encompassed mixing times ranging from ~5 ms to 10 000 ms, thanks to a confined impinging jet mixer [40]. The mixing cell was fed with two opposed jets, one of a solution of an amphiphilic diblock poly(butylacrylate)-b-poly(acrylic acid) (PBA(59)-b-PAA(104)) copolymer in methanol, the other of water. The mixing time for the two phases was controlled by the velocity of the jets. The sudden drop in solvent quality for the hydrophobic PBA blocks entailed rapid self-assembly of these blocks, inducing nucleation and growth of monodisperse spherical aggregates. The growth process was arrested by a corona brush of hydrophilic blocks covering the NPs. Johnson and Prud'homme have evidenced two regimes for the variation of NP size as a function of the mixing time: as the mixing time decreased, the NP size also decreased until a breakpoint, beyond which the particle size remained constant. At this breakpoint the mixing time τ_{mix} and aggregation time τ_{ag} were equivalent. This characteristic aggregation time decreased from 60 to 26 ms when the copolymer concentration in methanol increased from 0.1 wt.% to 0.65 wt.%. At very short mixing times, the time corresponding to the formation of NPs decreased with increasing initial concentration of polymer but the NP size was independent of the concentration. At larger mixing times, increasing the polymer concentration in the organic phase increased the mean size of the resulting particles (Fig. 7).

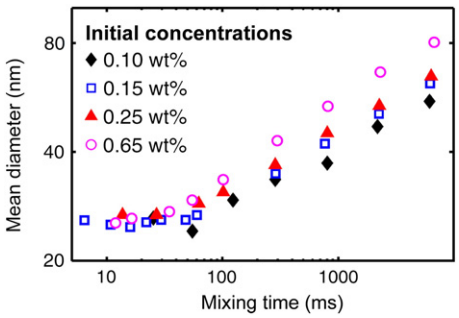

Fig. 7. Mean diameter of PBA(59)-b-PAA(104) nanoparticles as a function of the water-solvent mixing time with different initial concentrations of polymer in methanol (0.10 wt.%, 0.15 wt.%, 0.25 wt.% and 0.65 wt.%), adapted from [40,62].

As emphasized by the authors, this mechanism of nanoprecipitation is fundamentally different from the self-assembly of dynamic copolymer micelles at equilibrium, characterized by a fast exchange of polymer chains. Nanoprecipitation generates kinetically frozen NPs, not in a thermodynamic equilibrium but long-lived. During nanoprecipitation, the NP size increases until the energy barrier for insertion of single chains (unimers) becomes too high which happens for an aggregation number smaller than the equilibrium value. This energy barrier depends on the magnitude of solvent quality change. It has been suggested that it is lower when water-solvent interdiffusion is not complete, explaining why the NP size increases with increasing mixing time for $\tau_{mix} > \tau_{ag}$. Larger NPs can form before being kinetically frozen. When $\tau_{mix} < \tau_{ag}$, the NP size may be expected to become independent of polymer concentration.

Reaching equilibrium would require further exchange of single chains between aggregates, involving a change in the number of aggregates. These two stages of aggregation, a fast nucleation and growth leading to metastable NPs followed by a slow equilibration process, have been observed by synchrotron SAXS with millisecond time resolution for another amphiphilic block copolymer poly(ethylene–propylene)–poly(ethylene oxide) (PEP–PEO) [64]. Aggregation was induced by very fast mixing (4.5 ms) of dilute copolymer solution with water using a stopped-flow apparatus. The fast initial aggregation (~5–20 ms) led to metastable NPs while in the slow last step (~10^3–10^5 ms) the NP aggregation number increased, as the thermodynamic equilibrium was approached. The growth process was based on insertion and exchange of unimers. The rate of exchange of chains between aggregates formed by block copolymers may vary in a very large range, depending on the system. The main parameters that influence the exchange rate are the length and chemical nature of the hydrophobic blocks and the interfacial tension between the hydrophobic blocks and water [65]. Control of the exchange kinetics is important when aggregates are used as nanocarriers for drug delivery [66].

Amphiphilic block copolymer NPs prepared by nanoprecipitation did not always display a spherical core formed by hydrophobic blocks surrounded by a shell of hydrophilic blocks (typically PEG blocks). Some of the hydrophilic blocks could be buried within the NP core rather than well segregated in the corona, especially at high polymer molecular weight when the length of the hydrophobic blocks was large compared to the length of the PEG blocks. This was mainly evidenced by the NP sizes larger than those estimated for micelles, based on the polymer molecular weights. Slower mixing during nanoprecipitation resulted in a higher proportion of PEG entrapment within the NP cores. In contrast, core–shell structures, reminiscent of micelles formed by small surfactants, have been obtained for PLA–PEG copolymers with low molecular weights [67,68,44,49].

Stepanyan et al. have recently proposed a universal relationship between the NP size and two parameters, the ratio of the mixing time to the aggregation time and the initial polymer concentration [62]. When the mixing time is greater than the aggregation time of collapsed chains, the NPs size depends mainly on the mixing time and the initial polymer concentration if the surfactant concentration is sufficient. The

NP diameter is predicted to display a 1/3 power law as a function of these parameters but is independent of the polymer molar mass. The nanoprecipitation of a PCL/acetone solution in a 1 wt.% Pluronic P127 aqueous solution was well described by this model. The predictions of the model of Stepanyan et al. were also supported by the experimental data of Johnson and Prud'homme [40].

In summary, stable suspensions of nearly monodisperse polymeric NPs can be obtained using spontaneous emulsification in a narrow domain of composition of the polymer/solvent/non-solvent (water) ternary mixture. The Ouzo domain, located between the binodal and spinodal curves, corresponds to dilute polymer solutions and large amounts of water. The formation of NPs is accounted for by a nucleation and growth mechanism in a supersaturated polymer solution in the presence of a stabilizing agent. Alternatively, hydrophilic blocks of amphiphilic copolymers may play the role of surfactant. The initial system consists of isolated polymer coils in the solvent. As the solvent quality drops upon rapid mixing with a large amount of water, the polymer coils collapse, then collide and stick together. In parallel, the stabilizing molecules adsorb on the NPs formed and stop their coalescence. The mixing time parameter is of critical importance for the final NP size. For typical experimental conditions, i.e. relatively slow mixing in the presence of a stabilizer, the final NP size increases with the initial polymer concentration but is independent of the polymer molar mass.

8. Examples of application of polymeric nanoparticles obtained by nanoprecipitation for the delivery of therapeutic molecules

Hydrophobic drugs have been incorporated into nanocarriers by co-precipitation of the polymer/drug solution into water. For example, poor water soluble paclitaxel and docetaxel have been loaded into PLGA NPs taking advantage of nanoprecipitation. NPs containing these potent antimitotic agents have shown lower toxicity and enhanced efficacy compared to micelle-based formulations using low molecular weight surfactants [69]. Bilati et al. proposed to extend the use of nanoprecipitation to the encapsulation of more hydrophilic molecules, e.g. proteins, by an accurate selection of the solvent and non-solvent. They have shown that PLGA and PLA NPs could be obtained by precipitation of a DMSO solution into alcohol, enabling the incorporation of proteins [70].

A versatile nanoparticulate platform has been recently designed via nanoprecipitation of poly(alkyl cyanoacrylate) (PACA) based copolymers in an aqueous solution [71]. The nanocarriers combined a PACA core, a PEG outer shell imparting colloidal stability and stealth properties, fluorescent properties provided by covalent linkage of a rhodamine B-based dye to the polymer backbone of some chains, and terminal ligands for specific active targeting (Fig. 8). Regarding potential cancer therapy applications, stealth characteristics allow the NPs to escape the RES system, thereby prolonging NP blood circulation and enhancing the EPR effect in tumors. This passive targeting can be improved by using ligands that selectively bind to receptors overexpressed on tumor cells. Biotin has been used as a ligand for specific recognition of different cancer cell lines (i.e., human breast carcinoma MCF-7 and murine lung cancer M109). The efficient internalization, via biotin-receptor mediated endocytosis, of fluorescent targeted NPs was evidenced by flow cytometry. The encapsulation of paclitaxel in these functionalized NPs has been achieved, leading to a specific anticancer activity against MCF-7 cells *in vitro*. The relevance of this platform was further demonstrated in the field of Alzheimer's disease (AD). NPs were functionalized with either curcumin derivatives, known for their potential role in the prevention and treatment of AD, or with a novel specific antibody, in order to bind not only the β-amyloid peptide 1–42 ($A\beta_{1-42}$) monomer, a biomarker of AD, but also the corresponding fibrils, usually located in AD brains. These NPs displayed strong affinity for both monomeric and fibrillar peptides. This versatile platform paves the way to multifunctional NPs, targeting different pathologies when functionalized with appropriate ligands and carrying different hydrophobic drugs in their

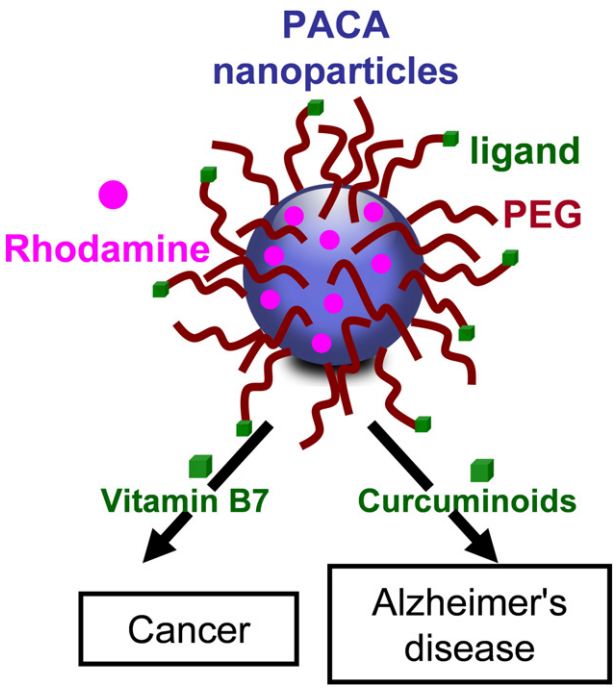

Fig. 8. Example of polymeric nanoparticles with a PACA core, a PEG outer shell, a rhodamine B-based dye and ligands for specific active targeting: vitamin B7 for specific recognition of different cancer cell lines or curcuminoids as ligands for abeta peptide, a marker of Alzheimer's disease (adapted from [71]).

PACA core. This holds great promise since PACA NPs alone have already shown significant preclinical results in different pathologies. Currently in phase III clinical trials, doxorubicin-loaded PACA NPs (i.e., Transdrug) improved survival, compared to the standard treatment, of patients with multidrug resistant hepatocarcinoma.

Besides NPs, the nanoprecipitation process also allowed the preparation of nanocapsules. A small amount of oil, in which an active compound could be dissolved, was added to the polymer solution. When this solution was rapidly mixed with water, core–shell NPs (or nanocapsules) were formed by precipitation of the hydrophobic polymer at the surface of oil droplets [57].

Natural phospholipids that self-assemble in liposomes have inspired to Discher and co-workers a new class of vesicles, termed polymersomes, made from amphiphilic diblock copolymers [72,73]. These polymer vesicles have been obtained by different methods, including nanoprecipitation. Aggregation was driven by the interaction between hydrophobic blocks, while the morphology was determined by the hydrophilic-to-hydrophobic volume fraction. Polymersomes were compared to viral capsids due to the high stability and low permeability of their shell. These properties were mainly correlated to the membrane thickness that could be modulated to a large extent by varying block lengths. Lecommandoux and co-workers have used a new generation of poly(g-benzyl L-glutamate)-block-hyaluronan (PBLG-b-HA), polypeptide–block–polysaccharide copolymers, to prepare polymersomes targeting overexpressed CD44 glycoprotein receptors in cancer cells, thanks to the hydrophilic hyaluronan moiety. Doxorubicine was successfully loaded in these polymersomes using co-precipitation and efficiently delivered to breast cancer cells (MCF-7) [46].

It is also worth mentioning a recent study of Bui et al., taking advantage in an original way of solvent shifting to self-assemble a capsid-like shell of block copolymer around a condensed complex of siRNA and polyethyleneimine (PEI) [74]. In the first step, branched PEI and siRNA were complexed in aqueous buffer, yielding positively charged NPs. These polyplexes were then dispersed in a DMSO-rich solution in which the amphiphilic hyaluronan-poly (g-benzyl-L-glutamate) block

copolymer was dissolved. Negatively charged hyaluronan moieties interacted with the preformed NPs via electrostatic interactions, giving rise to a surface monolayer of adsorbed copolymer. Excess copolymer chains in solution coexisted with adsorbed ones. In a last step, a large amount of water was added to this suspension, so that the solution became a non-solvent for the highly hydrophobic PBLG moieties, resulting in the self-assembly of isolated copolymer chains with chains adsorbed on the NPs. Hydrophobic interactions between the PBLG blocks allowed the formation of a copolymer bilayer membrane around the core of siRNA–PEI complexes (Fig. 9). This nanoconstruct mimicking the morphology of a virus showed a higher gene silencing activity than the PEI–siRNA complex alone.

These few illustrative examples show the important contribution of the nanoprecipitation/Ouzo effect to the design of nanocarriers for drug delivery and targeting.

9. Terpenoids-based nanoparticles: a new platform for theranostics

Drug-loaded NPs represent an attractive strategy for the treatment of severe diseases, especially in the field of cancer. However, increasing drug loading, usually less than 5–10 wt.%, remains a challenge and NPs often exhibit the so-called "burst release", in which a significant fraction of the cargo, generally corresponding to molecules simply adsorbed (or anchored) at the surface of the nanocarrier, is rapidly released upon parenteral administration.

Building nanocarriers with molecules covalently bound to the drug by a cleavable linkage (prodrug approach) may help to overcome these limitations [75]. A recent breakthrough has been achieved by Couvreur and co-workers who designed a unique and versatile platform for drug delivery, taking also advantage of the Ouzo effect. It consists in linking an isoprenoid chain to a biologically active drug molecule. Nanoassemblies of the bioconjugate are then obtained by nanoprecipitation without the need of any surfactant. Isoprenoid chains were chosen because isoprene is the basic structural motif of naturally occurring terpenoids which are extraordinary diverse in chemistry, structure and function. Among them, squalene is an acyclic triterpene, widespread in nature. In humans it is a precursor of the cholesterol biosynthesis.

The proof of concept of this nanoprodrug approach has been provided using the squalene as polyterpenoid moiety and gemcitabine as a model anticancer nucleoside analogue [76,77]. Gemcitabine is a fluorinated cytidine analogue used in clinic against various solid tumors and also active against lymphoid and myeloid cancer cell lines. However, its therapeutic potential is restricted by a poor stability in vivo, a limited intracellular diffusion and the induction of resistance. To overcome these drawbacks, squalene was covalently coupled to the amine function of gemcitabine, giving the 4-(N)-tris-nor-squalenoyl–gemcitabine bioconjugate (Sq–Gem) (Fig. 10a). This prodrug self-assembled in water as NPs with a diameter of about 120–140 nm. After intravenous administration, these Sq–Gem nanoassemblies, with a drug loading of almost 50% w/w, exhibited impressively higher anticancer activity than gemcitabine against both solid subcutaneously grafted tumors (panc-1, L1210 wt and P388) and aggressive metastatic leukemia (L1210 wt, P388 and RNK-16 LGL). This concept was then applied to other nucleosides or nucleosides analogues such as ddC, ddI, thymidine or adenosine. Remarkably, whatever the nucleosidic headgroup, the squalene-based bioconjugates spontaneously formed Nps upon nanoprecipitation of ethanolic solutions in water. These NPs exhibited a variety of supramolecular structures (ie. lamellar, inverse bicontinuous cubic or inverse hexagonal phases) [78–80].

The significant improvement in the activity of gemcitabine when coupled to squalene has led to extend the concept of squalenoylation to other drugs such as paclitaxel and penicillin G [81,82]. Unlike the amphiphilic nucleosidic bioconjugates, the hydrophobic squalenoyl–paclitaxel and squalenoyl–penicillin G conjugates self-assembled upon nanoprecipitation as dense spherical NPs devoid of internal structure (Fig. 10b). Squalenoyl–paclitaxel NPs showed antitumor efficacy

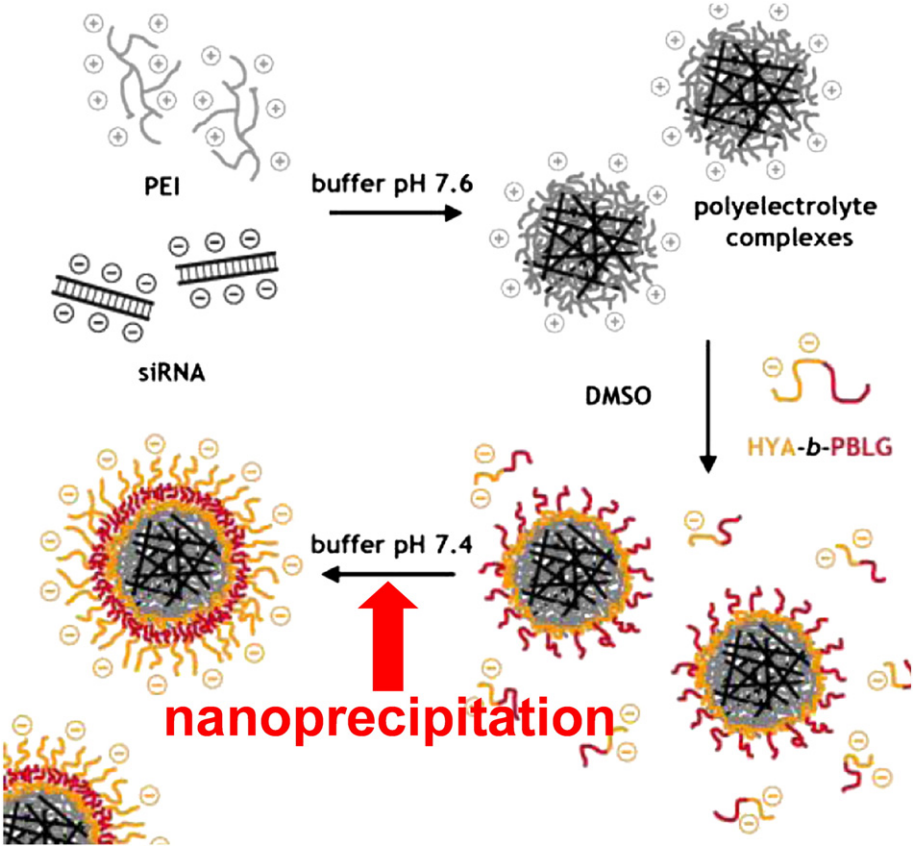

Fig. 9. Design of virus-like polymer nanoparticles by self-assembly of amphiphilic block copolymer molecules around siRNA-based polyelectrolyte complexes (reprinted from [74]).

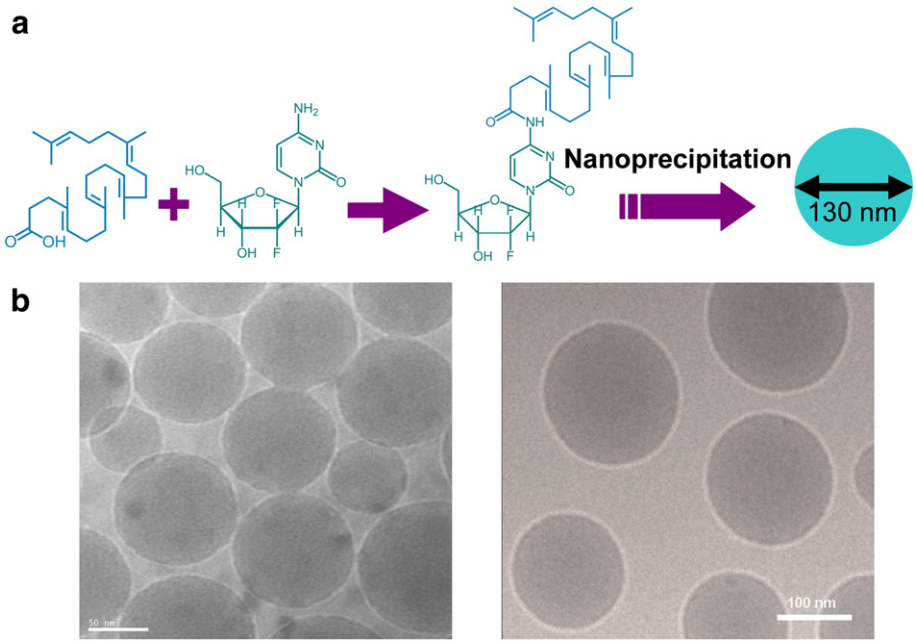

Fig. 10. (a). Squalenic acid coupled with gemcitabine molecules spontaneously self-assemble in water by nanoprecipitation, and form nanoparticles with a mean diameter (d) around 130 nm. (b). Selected Cryo-Tem images of squalenoyl–paclitaxel nanoparticles (left: d = 142 nm, PdI = 0.073) and squalenoyl–penicillin G (right: d = 140 nm, PdI = 0.1). Nanoparticles are dense spheres (adapted from [81,82]).

comparable to that of the parent drug but with much lower toxicity. Squalenoyl–penicillin G NPs increased the antibacterial activity of penicillin G against *Staphylococcus aureus* infection of macrophages thanks to their cell internalization through the endocytic pathways. Both these NPs were very stable and fairly monodisperse. Their colloidal stability could be correlated to their negative zeta potential (~−20 mV) and the insolubility of the conjugates, thus hindering Ostwald ripening. Interestingly, it was found that the initial concentration of the squalenoyl–paclitaxel in ethanol was a crucial parameter to control the final size of the NPs; the higher the concentration in ethanol, the smaller the size of the NPs. This trend is consistent with a nucleation and growth mechanism: as the number of nuclei varies exponentially with the supersaturation, higher solute concentrations are expected to yield higher numbers of nuclei and, therefore, smaller NPs if nuclei grow by capturing surrounding solute molecules.

Further studies focused on systematic modulation of the chain length used for the conjugation of gemcitabine. Either natural or synthesized terpenes, with a number of isoprenyl units varying from 1 to 6, were coupled to gemcitabine and the ability of the resulting bioconjugates to form NPs was assessed [83]. All the compounds yielded nanoassemblies active against several cancer cell lines but the prodrugs displaying a short hydrophobic chain precipitated soon after NP formation in the absence of stabilizer, upon ethanol evaporation. Ostwald ripening could be involved in the instability of the NP suspensions prepared with the shorter isoprene moieties.

Beyond short chains, well defined polyisoprene–gemcitabine conjugates were obtained by a living radical polymerization technique [84]. This method allowed the growth of polyisoprene chains of controlled molar mass with a gemcitabine moiety attached to one of the extremities of the polymer chains by a hydrolysable amide linkage. Upon nanoprecipitation in water from a THF solution, these conjugates formed NPs with a high payload ($W_{gem}/M_{n,PI}$) of gemcitabine, ranging from 10.5 wt.% for $M_{n,PI}$ = 2510 g/mol to 31.2 wt.% for $M_{n,PI}$ = 840 g/mol. The NPs size (~137 nm in diameter) did not show significant dependence on PI molar mass for Mn varying between 1190 g/mol and 2510 g/mol. The remarkable colloidal stability of the suspensions could be explained by the negative zeta potential of NPs (~−68 mV) and by the likely very low water solubility of PI–gem conjugates. The PI–gem NPs exhibited efficient anticancer activity both in vitro, on various cancer cell lines, and in vivo, on human pancreatic carcinoma-bearing mice while suppressing the inherent toxicity of gemcitabine. Noteworthy, the *in vivo* anticancer activity of the PI–gem conjugate increased with increasing PI molar mass.

The squalene-based platform for drug delivery has further been endowed with both magnetic responsiveness and imaging capabilities to combine diagnostic and therapeutic activities [85]. Multifunctional nanocarriers were prepared by one-step nanoprecipitation of a squalenoyl bioconjugate solution containing magnetite nanocrystals (USPIO). The USPIO/Sq–gem nanocomposites, injected to mice bearing the L1210 wt subcutaneous tumor model, could be guided by an external magnetic field toward the tumor tissue where they could be tracked by magnetic resonance imaging (MRI). To extend this theranostic concept to other contrast agents for MRI, nanocomposites associating Sq–Gem and a gadolinium Gd^{3+} contrast agent coupled to squalene were also designed.

10. Conclusion

Nanoprecipitation is a general strategy for obtaining a diversity of colloidal particles such as polymeric or lipidic nanospheres, nanocapsules, nanovesicules… It has also been used for the design of terpenoid-based nanoprodrugs. It may enable the preparation of fine dispersions of poorly water soluble, or even insoluble, pharmaceutical organic compounds, thus improving their bioavailability. The simplicity of the process and versatility of the materials that can be used have also given a decisive impulse to the design of nanocarriers intended for parenteral drug delivery. For the purpose of nanomedicine, the size distribution of NPs needs to be accurately controlled, which can be achieved taking advantage of the “Ouzo effect”. This spontaneous process does not require a precursor emulsion and generates a dispersion of quasi-monodisperse nanoparticles. The key factors controlling the formation of nanoparticles have been discussed but unsolved issues remain. NP characteristics are not determined only by the composition of the ternary system in a metastable state. The “Ouzo effect” and nanoprecipitation are strongly related to the kinetics of mixing of the organic solution containing the hydrophobic compound and the non-solvent, giving rise to supersaturated systems. Few experimental studies or simulations exist on the phenomena taking place during turbulent

or laminar mixing of the two phases which triggers particle formation. Furthermore, it is hard to investigate the early stages of NP formation because of the short time scales along with the small space scales of the process. The underlying mechanisms are often inferred from the dependence of final NP characteristics on experimental parameters. Specifically, the question of spinodal decomposition in systems containing small hydrophobic molecules at high supersaturation remains. Kinetic studies using synchrotron X-ray scattering might allow testing the mechanisms of NP formation and growth despite the limited scattering contrast between water and organic compounds. Little is known about co-precipitation of different compounds, either to load drug into nanocarriers or to arrest growth of NPs and to stabilize them. Co-precipitation of drugs and polymers influences drug loading into nanocarriers and NP size distribution. Investigation of the effects of amphiphilic block copolymer properties on NP stability should be extended. Residual solvent, as well as additives and drugs, could also interfere with the particle formation and stabilization processes. There is therefore an urgent need for further experiments and simulations in all these domains.

Part of the results disclosed in this review was supported by the European Research Council under the European Community's Seventh Framework Program FP7/ 2007–2013 (Grant Agreement no 249835).

References

[1] T.M. Allen, P.R. Cullis, Drug delivery systems: entering the main stream, Science 303 (2004) 1818–1822.
[2] J. Nicolas, S. Mura, D. Brambilla, N. Mackiewicz, P. Couvreur, Design, functionalization strategies and biomedical applications of targeted biodegradable/biocompatible polymer-based nanocarriers for drug delivery, Chem. Soc. Rev. 42 (2013) 1147–1235.
[3] E. Soussan, S. Cassel, M. Blanzat, I. Rico-Lattes, Drug delivery by soft matter: matrix and vesicular carriers, Angew. Chem. 48 (2009) 274–288.
[4] C. Vauthier, P. Couvreur, Nanomedicines: a new approach for the treatment of serious diseases, J. Biomed. Nanotechnol. 3 (2007) 1–12.
[5] L. Brannon-Peppas, J.O. Blanchette, Nanoparticle and targeted systems for cancer therapy, Adv. Drug Deliv. Rev. 56 (2004) 1649–1659.
[6] J. Panyam, V. Labhasetwar, Biodegradable nanoparticles for drug and gene delivery to cells and tissue, Adv. Drug Deliv. Rev. 55 (2003) 329–347.
[7] K. Kataoka, A. Harada, Y. Nagasaki, Block copolymer micelles for drug delivery: design, characterization and biological significance, Adv. Drug Deliv. Rev. 47 (2001) 113–131.
[8] H. Hillaireau, P. Couvreur, Nanocarriers' entry into the cell: relevance to drug delivery, Cell. Mol. Life Sci. 66 (2009) 2873–2896.
[9] H. Lee, H. Fonge, B. Hoang, R.M. Reilly, C. Allen, The effects of particle size and molecular targeting on the intratumoral and subcellular distribution of polymeric nanoparticles, Mol. Pharm. 7 (2010) 1195–1208.
[10] F. Lu, S.H. Wu, Y. Hung, C.Y. Mou, Size effect on cell uptake in well-suspended, uniform mesoporous silica nanoparticle, Small 5 (2009) 1408–1413.
[11] E.A. Simone, T.D. Dziubla, V.R. Muzykantov, Polymeric carriers: role of geometry in drug delivery, Expert Opin. Drug Deliv. 5 (2008) 1283–1300.
[12] D. Hühn, K. Kantner, C. Geidel, S. Brandholt, I. De Cock, S.J.H. Soenen, P. Rivera-Gil, J.M. Montenegro, K. Braeckmans, K. Müllen, G.U. Nienhaus, M. Klapper, W.J. Parak, Polymer-coated nanoparticles interacting with proteins and cells: focusing on the sign of the net charge, ACS Nano 7 (2013) 3253–3263.
[13] M.A. Dobrovolskaia, P. Aggarwal, J.B. Hall, S.E. McNeil, Preclinical studies to understand nanoparticle interaction with the immune system and its potential effects on nanoparticle biodistribution, Mol. Pharm. 5 (2008) 487–495.
[14] Y. Qiu, Y. Liu, L. Wang, L. Xu, R. Bai, Y. Ji, X. Wu, Y. Zhao, Y. Li, C. Chen, Surface chemistry and aspect ratio mediated cellular uptake of Au nanorods, Biomaterials 31 (2010) 7606–7619.
[15] P. Decuzzi, R. Pasqualini, W. Arap, M. Ferrari, Intravascular delivery of particulate systems: does geometry really matter? Pharm. Res. 26 (2009) 235–243.
[16] H. Maeda, J. Wu, T. Sawa, Y. Matsumura, K. Hori, Tumor vascular permeability and the EPR effect in macromolecular therapeutics: a review, J. Control. Release 65 (2000) 271–284.
[17] H. Maeda, Macromolecular therapeutics in cancer treatment: the EPR effect and beyond, J. Control. Release 164 (2012) 138–144.
[18] F. Yuan, M. Dellian, D. Fukumura, M. Leuning, D.D. Berk, V.P. Yorchilin, R.K. Jain, Vascular permeability in a human tumor xenograft : molecular size dependence and cutoff size, Cancer Res. 55 (1995) 3752–3756.
[19] V.P. Torchilin, Targeted pharmaceutical nanocarriers for cancer therapy and imaging, AAPS J. 9 (2007)(article 15).
[20] C. Vauthier, K. Bouchemal, Methods for the preparation and manufacture of polymeric nanoparticles, Pharm. Res. 26 (2009) 1025–1056.
[21] S. Galindo-Rodriguez, E. Alleman, H. Fessi, E. Doelker, Physicochemical parameters associated with nanoparticle formation in the salting-out, emulsification–diffusion, and nanoprecipitation methods, Pharm. Res. 21 (2004) 1428–1439.
[22] C.E. Mora-Huertas, H. Fessi, A. Elaissari, Influence of process and formulation parameters on the formation of submicron particles by solvent displacement and emulsification–diffusion methods. Critical comparison, Adv. Colloid Interf. Sci. 163 (2011) 90–122.
[23] S.A. Vitale, J.L. Katz, Liquid droplet dispersions formed by homogeneous liquid–liquid nucleation: "the Ouzo effect", Langmuir 19 (2003) 4105–4110.
[24] F. Ganachaud, J.L. Katz, Nanoparticles and nanocapsules created using the Ouzo effect: spontaneous emulsification as an alternative to ultrasonic and high-shear devices, ChemPhysChem 9 (2005) 209–216.
[25] D. Horn, J. Rieger, Organic nanoparticles in aqueous phase, Angew. Chem. 40 (2001) 4330–4361.
[26] J. Aubry, F. Ganachaud, J.P. Cohen-Addad, B. Cabane, Nanoprecipitation of polymethylmethacrylate by solvent shifting: 1. Boundaries, Langmuir 25 (2009) 1970–1979.
[27] M.A. Watzky, R.G. Finke, Transition metal nanocluster formation kinetic and mechanistic studies. A new mechanism when hydrogen is the reductant: slow, continuous nucleation and fast autocatalytic surface growth, J. Am. Chem. Soc. 119 (1997) 10382–10400.
[28] J. Han, F. Testard, F. Maloggi, P.E. Coulon, N. Menguy, O. Spalla, Understanding of the size control of biocompatible gold nanoparticles in millifluidic channels, Langmuir 28 (2012) 15966–15974.
[29] E. Matijevic, Uniform inorganic colloid dispersions. Achievements and challenges, Langmuir 10 (1994) 8–16.
[30] J. Polte, T.T. Ahner, F. Delissen, S. Sokolov, F. Emmerling, A.F. Thünemann, R. Kraehnert, Mechanism of gold nanoparticle formation in the classical citrate synthesis method derived from coupled in situ XANES and SAXS evaluation, J. Am. Chem. Soc. 132 (2010) 1296–1301.
[31] J. Polte, R. Erler, A.F. Thünemann, S. Sokolov, T.T. Ahner, K. Rademann, F. Emmerling, R. Kraehnert, Nucleation and growth of gold nanoparticles studied via in situ small angle X-ray scattering at millisecond time resolution, ACS Nano 4 (2010) 1076–1082.
[32] Y. Liu, K. Kathan, W. Saad, R.K. Prud'homme, Ostwald ripening of β-carotene nanoparticles, Phys. Rev. Lett. 98 (2007) 036102.
[33] R. Botet, The "Ouzo effect", recent developments and application to therapeutic drug carrying, J. Phys. Conf. Ser. 352 (2012) 1–8.
[34] D. Carteau, I. Pianet, P. Brunerie, B. Guillemat, D.M. Bassani, Probing the initial events in the spontaneous emulsification of trans-anethole using dynamic NMR spectroscopy, Langmuir 23 (2007) 3561–3565.
[35] D. Carteau, D. Bassani, I. Pianet, The «Ouzo effect»: following the spontaneous emulsification of trans-anethole in water by NMR, C.R. Chim. 11 (2008) 493–498.
[36] I. Grillo, Small-angle neutron scattering study of a world-wide known emulsion: Le Pastis, Colloids Surf., A 225 (2003) 153–160.
[37] N.L. Sitnikova, R. Sprik, G. Wegdam, E. Eiser, Spontaneously formed trans-anethol/water/alcool emulsions: mechanism of formation and stability, Langmuir 21 (2005) 7083–7089.
[38] E. Scholten, E. van der Linden, H. This, The life of an anise flavored alcoholic beverage: does its stability cloud or confirm theory? Langmuir 24 (2008) 1701–1706.
[39] V. Kumar, R.K. Prud'homme, Nanoparticle stability: processing pathways for solvent removal, Chem. Eng. Sci. 64 (2009) 1358–1361.
[40] B.K. Johnson, R.K. Prud'homme, Mechanism for rapid self-assembly of block copolymer nanoparticles, Phys. Rev. Lett. 91 (2003) 118302.
[41] P.C. Hiemenz, R. Rajagopalan, Principles of Colloid and Surface Chemistry, 3rd edition Marcel Dekker Inc., New York, 1997.
[42] K. Roger, R. Botet, B. Cabane, Coalescence of repelling colloidal droplets: a route to monodisperse populations, Langmuir 29 (2013) 5689–5700.
[43] Z. Zhu, K. Margulis-Goshen, S. Magdassi, Y. Talmon, C.W. Macosko, Polyelectrolyte stabilized drug nanoparticles via flash nanoprecipitation: a model study with β-carotene, J. Pharm. Sci. 99 (2010) 4295–4306.
[44] Z. Zhu, Effects of amphiphilic diblock copolymer on drug nanoparticle formation and stability, Biomaterials 34 (2013) 10238–10248.
[45] H. Lannibois, A. Hasmy, R. Botet, O. Aguerre Charriol, B. Cabane, Surfactant limited aggregation of hydrophobic molecules in water, J. Phys. II France 7 (1997) 319–342.
[46] K.K. Upadhyay, A.N. Bhatt, A.K. Mishra, B.S. Dwarakanath, S. Jain, C. Schatz, J.F. Le Meins, A. Farooque, G. Chandraiah, A.K. Jain, A. Misra, S. Lecommandoux, The intracellular drug delivery and anti tumor activity of doxorubicin loaded poly(gamma-benzyl L-glutamate)-b-hyaluronan polymersomes, Biomaterials 31 (2010) 2882–2892.
[47] R. Campardelli, G. Della Porta, E. Reverchon, Solvent elimination from polymer nanoparticle suspensions by continuous supercritical extraction, J. Supercrit. Fluids 70 (2012) 100–105.
[48] S.M. d'Addio, R.K. Prud'homme, Controlling drug nanoparticle formation by rapid precipitation, Adv. Drug Deliv. Rev. 63 (2011) 417–426.
[49] R. Karnik, F. Gu, P. Basto, C. Cannizaro, L. Dean, W. Kyei-Manu, R. Langer, O.C. Farokhzad, Microfluidic platform for controlled synthesis of polymeric nanoparticles, Nano Lett. 8 (2008) 2906–2912.
[50] B.K. Johnson, R.K. Prud'homme, Chemical processing and micromixing in confined impinging jets, AIChE J. 49 (2003) 2264–2282.
[51] Y. Liu, R.O. Fox, CFD predictions for chemical processing in a confined impinging-jets reactor, AIChE J. 52 (2006) 731–744.
[52] F. Bally, D.K. Garg, C.A. Serra, Y. Hoarau, N. Anton, C. Brochon, D. Parida, T. Vandamme, G. Hadziioannou, Improved size-tunable preparation of polymeric nanoparticles by microfluidic nanoprecipitation, Polymer 53 (2012) 5045–5051.
[53] J. Molpeceres, M. Guzman, M.R. Arberturas, M. Chacon, L. Berges, Application of central composite designs to the preparation of polycaprolactone nanoparticles by solvent displacement, J. Pharm. Sci. 85 (1996) 206–213.

[54] B. Abecassis, F. Testard, O. Spalla, P. Barboux, Probing in situ the nucleation and growth of gold nanoparticles by small-angle X-ray scattering, Nano Lett. 7 (2007) 1723–1727.
[55] M.C. Brick, H.J. Palmer, T.H. Whitesides, Formation of colloidal dispersions of organic materials in aqueous media by solvent shifting, Langmuir 19 (2003) 6367–6380.
[56] H. Haberkorn, D. Franke, Th. Frechen, W. Goesele, J. Rieger, Early stages of particle formation in precipitation reactions — quinacridone and boehmite as generic examples, J. Colloid Interface Sci. 259 (2003) 112–126.
[57] H. Fessi, F. Puisieux, J.P. Devissaguet, N. Ammoury, S. Benita, Nanocapsule formation by interfacial polymer deposition following solvent displacement, Int. J. Pharm. 55 (1989) R1–R4.
[58] O. Thioune, H. Fessi, J.P. Devissaguet, F. Puisieux, Preparation of pseudolatex by nanoprecipitation: influence of the solvent nature on intrinsic viscosity and interaction constant, Int. J. Pharm. 146 (1997) 233–238.
[59] S. Stainmesse, A.-M. Orecchioni, E. Nakache, F. Puisieux, H. Fessi, Formation and stabilization of a biodegradable polymeric colloidal suspension of nanoparticles, Colloid Polym. Sci. 273 (1995) 505–511.
[60] M. Beck-Broichsitter, E. Rytting, T. Lebhardt, X. Wang, T. Kissel, Preparation of nanoparticles by solvent displacement for drug delivery: a shift in the "Ouzo region" upon drug loading, Eur. J. Pharm. Sci. 41 (2010) 244–253.
[61] P. Legrand, S. Lesieur, A. Bochot, R. Gref, W. Raatjes, G. Barratt, C. Vauthier, Influence of polymer behaviour in organic solution on the production of polylactide nanoparticles by nanoprecipitation, Int. J. Pharm. 344 (2007) 33–43.
[62] R. Stepanyan, J.G.J.L. Lebouille, J.J.M. Slot, R. Tuinier, M.A. Cohen Stuart, Controlled nanoparticle formation by diffusion limited coalescence, Phys. Rev. Lett. 109 (2012) 138301.
[63] J. Cheng, B.A. Teply, I. Sherifi, J. Sung, G. Luther, F.X. Gu, E. Levy-Nissenbaum, A.F. Radovic-Moreno, R. Langer, O.C. Farokhzad, Formulation of functionalized PLGA–PEG nanoparticles for in vivo targeted drug delivery, Biomaterials 28 (2007) 869–876.
[64] R. Lund, L. Willner, M. Monkenbusch, P. Panine, T. Narayanan, J. Colmenero, D. Richter, Structural observation and kinetic pathway in the formation of polymeric micelles, Phys. Rev. Lett. 102 (2009) 188301.
[65] T. Nicolai, O. Colombani, C. Chassenieux, Dynamic polymeric micelles versus frozen nanoparticles formed by block copolymers, Soft Matter 6 (2010) 3111–3118.
[66] V. Kumar, L. Wang, M. Riebe, H.H. Tung, R.K. Prud'homme, Formulation and stability of Itraconazole and Odanacatib nanoparticles: governing physical parameters, Mol. Pharm. 6 (2009) 1118–1124.
[67] T. Riley, S. Stolnik, C.R. Heald, C.D. Xiong, M.C. Garnett, L. Illum, S.S. Davis, S.C. Purkiss, R.J. Barlow, P.R. Gellert, Physicochemical evaluation of nanoparticles assembled from poly(lactic acid)–poly(ethylene glycol) (PLA–PEG) block copolymers as drug delivery vehicles, Langmuir 17 (2001) 3168–3174.
[68] Z. Zhu, J.L. Anacker, S. Ji, T.R. Hoye, C.W. Macosko, R.K. Prud'homme, Formation of block copolymer-protected nanoparticles via reactive impingement mixing, Langmuir 23 (2007) 10499–10504.
[69] G. Gaucher, R.H. Marchessault, J.C. Leroux, Polyester-based micelles and nanoparticles for the parenteral delivery of taxanes, J. Control. Release 143 (2010) 2–12.
[70] U. Bilati, E. Allemann, E. Doelker, Development of a nanoprecipitation method intended for the entrapment of hydrophilic drugs in nanoparticles, Eur. J. Pharm. Sci. 24 (2005) 67–75.
[71] B. Le Droumaguet, J. Nicolas, D. Brambilla, S. Mura, A. Maksimenko, L. De Kimpe, E. Salvati, C. Zona, C. Airoldi, M. Canovi, M. Gobbi, M. Noiray, B. La Ferla, F. Nicotra, W. Scheper, O. Flores, M. Masserini, K. Andrieux, P. Couvreur, Versatile and efficient targeting using a single nanoparticulate platform: application to cancer and Alzheimer's disease, ACS Nano 6 (2012) 5866–5879.
[72] B.M. Discher, Y.Y. Won, D.S. Ege, J.C.M. Lee, F.S. Bates, D.E. Discher, D.A. Hammer, Polymersomes: though vesicles made from diblock copolymers, Science 284 (1999) 1143–1146.
[73] D.E. Discher, A. Eisenberg, Polymer vesicles, Science 297 (2002) 967–973.
[74] L. Bui, S. Abbou, E. Ibarboure, N. Guidolin, C. Staedel, J.J. Toulme, S. Lecommandoux, C. Schatz, Encapsidation of RNA–polyelectrolyte complexes with amphiphilic block copolymers: toward a new self-assembly route, J. Am. Chem. Soc. 134 (2012) 20189–20196.
[75] M.J. Joralemon, S. McRae, T. Emrick, PEGylated polymers for medicine: from conjugation to self-assembled systems, Chem. Commun. 46 (2010) 1377–1393.
[76] P. Couvreur, B. Stella, L.H. Reddy, H. Hillaireau, C. Dubernet, D. Desmaële, S. Lepêtre-Mouelhi, F. Rocco, N. Dereudre-Bosquet, P. Clayette, V. Rosilio, V. Marsaud, J.M. Renoir, L. Cattel, Squalenoyl nanomedicines as potential therapeutics, Nano Lett. 6 (2006) 2544–2548.
[77] P. Couvreur, L.H. Reddy, S. Mangenot, J.H. Poupaert, D. Desmaële, S. Lepêtre-Mouelhi, B. Pili, C. Bourgaux, H. Amenitsch, M. Ollivon, Discovery of new hexagonal supramolecular nanostructures formed by squalenoylation of an anticancer nucleoside analogue, Small 4 (2008) 247–253.
[78] V. Allain, C. Bourgaux, P. Couvreur, Self-assembled nucleolipids: from supramolecular structure to soft nucleic acid and drug delivery devices, Nucleic Acids Res. 40 (2012) 1891–1903.
[79] E. Lepeltier, C. Bourgaux, V. Rosilio, J.H. Poupaert, F. Meneau, F. Zouhiri, S. Lepêtre-Mouelhi, D. Desmaële, P. Couvreur, Self-assembly of squalene-based nucleolipids: relating the chemical structure of the bioconjugates to the architecture of the nanoparticles, Langmuir 29 (2013) 14795–14803.
[80] F. Bekkara-Aounallah, R. Gref, M. Othman, L.H. Reddy, B. Pili, V. Allain, C. Bourgaux, H. Hillaireau, S. Lepêtre-Mouelhi, D. Desmaële, J. Nicolas, N. Chafi, P. Couvreur, Novel PEGylated nanoassemblies made of self-assembled squalenoyl nucleoside analogues, Adv. Funct. Mater. 18 (2008) 3715–3725.
[81] J. Caron, A. Maksimenko, S. Wack, E. Lepeltier, C. Bourgaux, E. Morvan, K. Leblanc, P. Couvreur, D. Desmaele, Improving the antitumoractivity of squalenoyl–paclitaxel conjugate nanoassemblies by manipulating the linker between paclitaxel and squalene, Adv. Healthc. Mater. 2 (2013) 172–185.
[82] N. Semiramoth, C. Di Meo, F. Zouhiri, F. Saïd-Hassane, S. Valetti, R. Gorges, V. Nicolas, J.H. Poupaert, S. Chollet-Martin, D. Desmaële, R. Gref, P. Couvreur, Self-assembled penicillin bioconjugates: an original approach for the treatment of intracellular infections, ACS Nano 6 (2012) 3820–3831.
[83] A. Maksimenko, J. Mougin, S. Mura, E. Sliwinski, E. Lepeltier, C. Bourgaux, S. Lepêtre, F. Zouhiri, D. Desmaële, P. Couvreur, Polyisoprenoyl gemcitabine conjugates self-assemble as nanoparticles, useful for cancer therapy, Cancer Lett. 334 (2013) 346–353.
[84] S. Harrisson, J. Nicolas, A. Maksimenko, D.T. Bui, J. Mougin, P. Couvreur, Nanoparticles with in vivo anticancer activity from polymer prodrug amphiphiles prepared by living radical polymerization, Angew. Chem. 52 (2013) 1678–1682.
[85] J.L. Arias, L.H. Reddy, M. Othman, B. Gillet, D. Desmaële, F. Zouhiri, F. Dosio, R. Gref, P. Couvreur, Squalene-based nanocomposites: a new platform for the design of multifunctional pharmaceutical theragnostics, ACS Nano 5 (2011) 1513–1521.